Int. J. Electrochem. Sci., 17 **(2022)** Article Number: 220732, doi: 10.20964/2022.07.26

International Journal of
ELECTROCHEMICAL
SCIENCE
www.electrochemsci.org

Degradation of a Reactive Orange 16 in textile wastewater treatment using CuO/ZnO nanocomposite as photocatalyst

Chao Luo[1,*], *Wanhe Yao*[2], *Xu Gao*[3]

[1] CenerTech Tianjin Chemical Research and Design Institute Co., Ltd., Tianjin 300131, China
[2] Cnooc Ningbo Daxie Petrochemical Ltd, Ningbo 315812, China
[3] PetroChina Guangxi Petrochemical Company, 535000, Qinzhou, China
[*]E-mail: cnooclc@sina.com

Received: 31 March 2022 / *Accepted:* 10 May 2022 / *Published:* 6 June 2022

In this study, photo-electrocatalytic degradation of Reactive Orange 16 (RO16) dye by CuO/ZnO nanocomposite under UV and sunlight irradiation for textile wastewater treatment was demonstrated. CuO/ZnO nanostructure was synthesized using a hydrothermal technique. The production of a monoclinic phase of leaf-shaped CuO loaded on a hexagonal wurtzite structure of rod-shaped ZnO was confirmed by FE-SEM and XRD investigations of the nanocomposite. According to optical experiments, the band gap energies of CuO, ZnO, and CuO/ZnO nanocomposite were 1.99, 2.19, and 3.34 eV, respectively. CuO/ZnO nanocomposite has effective charge separation and faster charge transfer than CuO and ZnO, according to an EIS investigation. In a photocatalytic investigation, the entire elimination of 150 ml of 100 mg/l RO16 solution was achieved after 160, 135 and 120 minutes of UV light illumination, and after 115, 140, and 100 minutes of sunlight illumination for CuO, ZnO, and CuO/ZnO nanocomposite, respectively. The results show that dye degradation is faster when exposed to sunlight than when exposed to UV radiation, which can be related to band gap engineering and the creation of interfacial contact between CuO and ZnO nanostructures in CuO/ZnO nanocomposite. In this study, the photocatalytic performance of the prepared photocatalysts was tested for degradation of actual samples prepared using textile wastewater under sunlight irradiation, and the results show that the CuO/ZnO nanocomposite has the appropriate capability to treat RO16 from textile wastewater.

Keywords: Leaf-shaped CuO; Rod-shaped ZnO; CuO/ZnO nanocomposite; Reactive Orange 16; Photodegradation; Textile wastewater

1. INTRODUCTION

Reactive Orange 16 (RO16), also known as Remazol Brilliant Orange 3R, is an azo chemical that is a 6-acetamido-4-hydroxy-3-[[4-(2-sulfonatooxyethylsulfonyl] phenyl] diazenyl] naphthalene-2-

sulfonate] [1]. RO16 is unique among reactive dyes in that it may covalently link to textile fibers and is resistant to degradation by traditional removal procedures [2-5]. RO16 has one or more sensitive atoms that allow it to react with amino acid functional groups and cellulose hydroxyl of synthetic fabrics [6, 7]. As a result, it is frequently employed in textile dyeing procedures for dyeing cotton, wool, viscose fiber, silk, leather, and nylon [8-11].

Toxic chemicals are released into the aquatic environment when dye-containing effluents are discharged into the water [12, 13]. It reduces sunlight penetration and lowers oxygen levels in water, resulting in major environmental and health consequences [14-16]. Reactive dyes become poisonous only after the azo linkage is reduced and cleaved to generate aromatic amines and toxic amines, posing health risks by damaging key organs such as the brain, liver, kidneys, central nervous system, and reproductive systems [17-19].

Accordingly, many methods such as chemical oxidation [20], adsorption [21], ozonation, coagulation [22], Fenton oxidation [23], reverse osmosis [24], biodegradation [25], membrane filtration [26], anion exchange [27], electrochemical degradation [28, 29] and photocatalytic degradation [30-38] have been investigated for the treatment of dye contaminated wastewater. Among them, the photocatalytic degradation process provides an attractive alternative for the treatment of dye-containing wastewater, and eco-friendly and low-cost photocatalysts have been employed for various organic and inorganic pollutants. Therefore, in this study, the photo-electrocatalytic degradation of RO16 dye was investigated by using a CuO/ZnO nanostructure under UV and sunlight irradiation.

2. EXPERIMENT

2.1. Synthesis of CuO/ZnO nanostructure

The CuO/ZnO nanostructure was synthesized using a hydrothermal technique [39]. 4 mL hydrazine hydrate (80%, Sigma-Aldrich) was combined with 50 mL aqueous solution of 0.05 M zinc acetate dihydrate (98%, Sigma-Aldrich). The mixture was agitated for 5 minutes before being autoclaved at 145°C for 24 hours in an 80 mL Teflon-lined stainless steel autoclave. The resultant white precipitate of ZnO was collected after cooling, washed three times with a mixture of deionized water and ethanol, and dried in an oven at 75 °C for 10 hours. The CuO/ZnO nanostructure was prepared by ultrasonically dispersing 0.5 g of manufactured ZnO and 0.1 g of acetate copper hydrate (99%, Sigma-Aldrich) in 100 mL of N,N-Dimethylformamide anhydrous (DMF, 99.8 percent , Sigma-Aldrich). Then, the dispersed mixture was stirred in a water bath at 85 °C for 4 hours. Subsequently, the mixture was centrifuged at 1000 rpm for 10 minutes, the precipitate was washed thoroughly with a mixture of deionized water and ethanol three times, and dried at 65 °C for 10 hours in an oven.

2.2. Characterization

The crystal structures and morphology of the produced nanostructures were studied using an X-ray diffractometer (XRD; Bruker D8 advance AXS GmbH, Karlsruhe, Germany) and field emission scanning electron microscopy (FE-SEM; Hitachi Company Model S-4160, China). A

spectrophotometer was used to record the UV-visible absorption spectra of the samples (Jasco-V 530, Japan). The electrochemical impedance spectroscopy (EIS) measurements were carried out in a three-electrode electrochemical system using a ZENNIUM electrochemical workstation (ZAHNER-elektrik GmbH & Co. KG, Germany) with a CuO or ZnO or CuO/ZnO nanocomposite modified glassy carbon electrode (GCE) as the working electrode, a platinum wire as the counter electrode, and Ag/AgCl as the reference electrode. EIS measurements were performed in a 0.5 M Na_2SO_4 (≥99.0%, Sigma-Aldrich) solution by applying an AC voltage of 10 mV in the frequency range from 10^{-2} Hz to 10^5 Hz at open circuit. The impedance data was modeled using the ZVIEW software package. For modification of the GCE, 0.7 ml of 0.8 g/l of synthesized nanostructures were dropped on the GCE, and the electrode was dried at room temperature.

2.3. Study the photocatalytic Activity

Under sunlight irradiation and equipped with UV light, photocatalytic degradation studies were carried out in a photoreactor with a neck pyrex flask type (Hebei Flash Cure Optoelectronic Technology Co., Ltd., China). 0.4 g/1 produced photocatalyst was added to 150 ml of 100 mg/l RO16 (70%, Sigma-Aldrich) solution. Before the measurements, the dye solution and photocatalyst suspension were magnetically agitated for one hour in the dark to achieve adsorption–desorption equilibrium. The RO16 solution was then degraded by exposing the suspension to sunshine or UV radiation. The distance between the light source's surface and the RO16 solution's surface was 10 cm. Decolorization of RO16 dye solutions was determined by measuring the absorbance of dye solutions at λ_{max} = 493 nm at different intervals by a UV–vis spectrophotometer (DR2800, Hach, USA), and degradation efficiency can be calculated by the following equation [40, 41]:

$$\text{Degradation efficiency (\%)} = \frac{I_0 - I_t}{I_0} \times 100$$

Where I_0 denotes the absorbance of the initial RO16 dye; I_t presents the absorbance of the dye solution after irradiation at time t.

3. RESULTS AND DISCUSSION

3.1. Study of morphology and structure of synthesized nanostructures

Figure 1 shows the XRD patterns of CuO, ZnO, and CuO/ZnO nanocomposite. Patterns from X-Ray Diffraction The characteristic peaks of CuO at 35.51°, 38.57°, 48.66°, 61.25°, and 66.55°, which are indexed to ($\bar{1}$11), (111), (2 02), (113), and (022) planes, are in agreement with those of the monoclinic phase of CuO standard patterns (JCPDS card no. 48-1548) [42-44]. As seen from the XRD pattern of ZnO nanostructures, there are diffraction peaks at 31.99°, 34.57°, 36.35°, 47.71°, 56.63°, 63.07°, 67.70° and 69.05° which are assigned to (100), (002), (101), (102), (110), (103), (112) and (201) planes of the hexagonal wurtzite structure of ZnO (JCPDS card no. 36–1451) [45, 46].

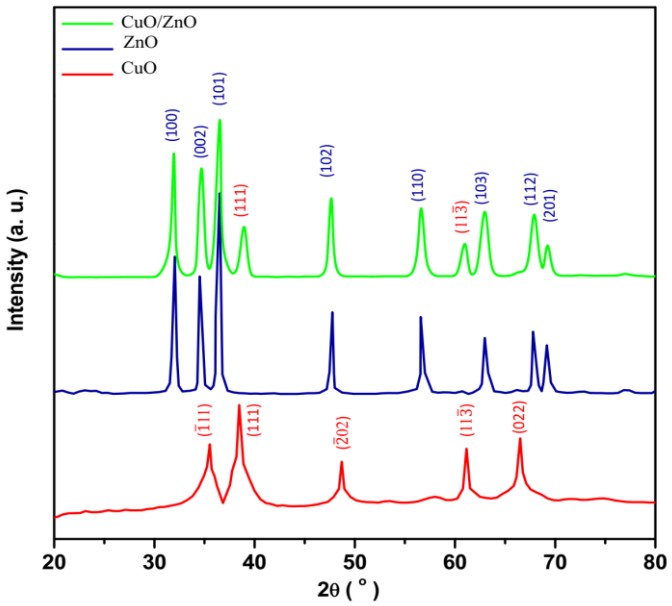

Figure 1. The XRD patterns of CuO, ZnO and CuO/ZnO nanocomposite.

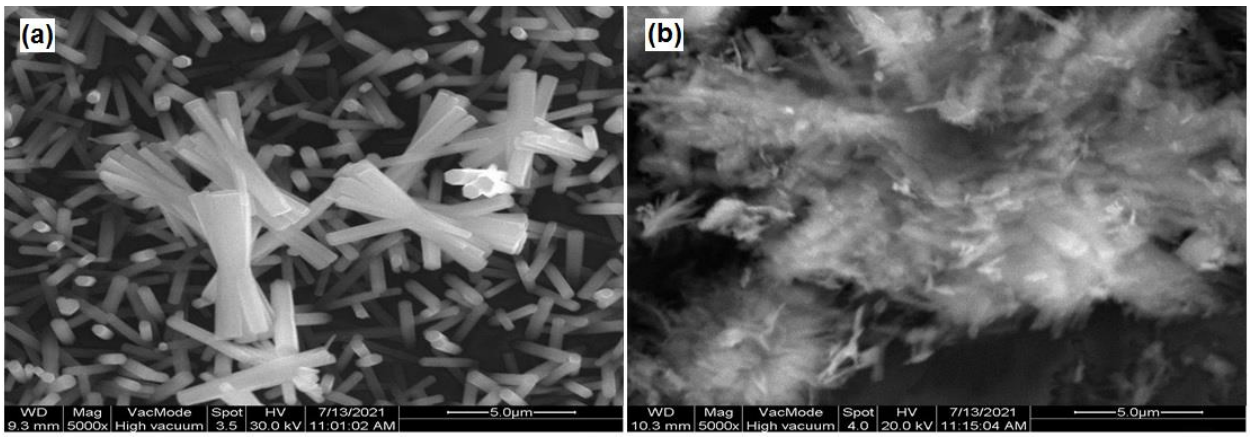

Figure 2. FE-SEM images of (a) ZnO and (b) CuO/ZnO nanocomposite.

The XRD pattern of the CuO/ZnO nanocomposite presents the diffraction peaks of hexagonal wurtzite ZnO and two additional diffraction peaks correspond to (111) and (11$\bar{3}$) reflections of the monoclinic phase of CuO, indicating the presence of CuO species on the ZnO structure [47, 48]. These results confirm the formation of CuO loaded ZnO hierarchical structures.

FE-SEM images of ZnO and CuO/ZnO nanocomposite are shown in Figure 2. Rod-shaped structures with an average diameter of 150 nm make up the ZnO sample. The CuO/ZnO nanocomposite heterostructure shown by FE-SEM images is a combination of leaf-shaped CuO and rod-shaped ZnO nanostructures. The combination of rod and leaf-shaped CuO/ZnO nanocomposite results in a rough and porous surface with multiple active sites on the nanocomposite's surface, increasing the effective surface area and photocatalytic activity [49-51].

3.2. Study of optical properties

Figure 3a shows the optical absorbance spectra of CuO, ZnO, and CuO/ZnO nanocomposite. The spectra of ZnO shows a notable absorption edge in the UV area (400 nm) and weak absorption in the visible light range, which is attributable to pure ZnO's intrinsic band-gap energy [52, 53]. The absorbance spectra of CuO illustrates the broad absorption feature in the visible-light wavelengths up to 800 nm, which is related to the visible-light absorption characteristics of CuO [54-57]. Meanwhile, the CuO/ZnO nanocomposite shows not only a broad range of absorption but also the highest optical absorption in comparison to that of the ZnO and the CuO nanostructures. The increased absorption of the CuO/ZnO nanocomposite in the visible region indicates the covering of the ZnO with CuO [58, 59]. This band gap absorption peak shifts to the lower wavelength side toward ZnO. When a wide band gap semiconductor is coupled with a narrow band gap semiconductor with a more negative conduction band level, the optical absorption abilities of the catalysts by extending the absorption range of the solar spectrum are enhanced [60-62], and separation of the photogenerated carriers under the internal field induced by the different electronic band structures of both semiconductors is facilitated because electrons from the conduction band of the narrow band gap semiconductor can be easily injected into the conduction band of the wide band gap semiconductor [63-65]. Moreover, the introduction of the ZnO with CuO enhances the absorbance and improves the carrier mobility because of the lattice distortion and impurity levels in the CuO/ZnO nanocomposite [66, 67]. As illustrated in Figure 3b, the band-gap energy (E) value can be determined from the intercept of the linear portion of the $(\alpha h\nu)^2$ versus photon energy ($h\nu$) to the energy axis, where α is the absorption coefficient, h is the Planck's constant (4.1357×10^{-15} eV.s), and ν is the light frequency [68-70]. CuO, ZnO, and CuO/ZnO nanocomposite have estimated band gap energies of 1.99, 2.19, and 3.34 eV, respectively. As a result, the decrease in band gap energy in the CuO/ZnO nanocomposite toward ZnO indicates that photo-excitation of charge carriers with low energy is facilitated, resulting in more electron and hole pairs and improved photocatalytic treatment of dyes.

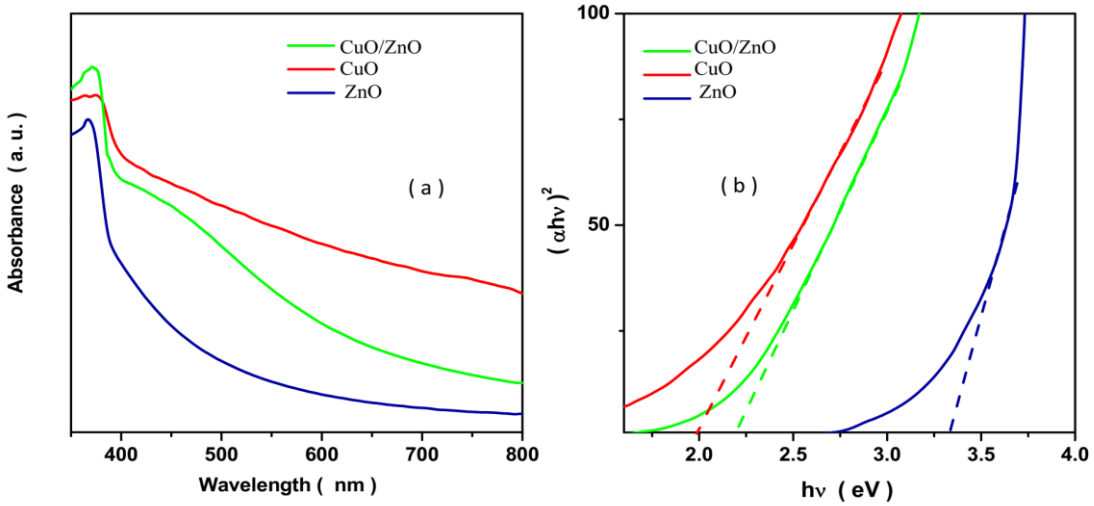

Figure 3. (a) Optical absorbance spectra and (b) plot of $(\alpha h\nu)^2$ versus photon energy ($h\nu$) of CuO, ZnO and CuO/ZnO nanocomposite at room temperature.

3.3. EIS study

Figures 4a and 4b show the Nyquist and Bode plots of CuO, ZnO, and CuO/ZnO nanocomposite modified GCE, respectively. The elements of the corresponding circuit models in Figure 4a were utilized to fit the experimental data and obtain the physical parameters listed in Table 1 of these results. R_s denotes the series resistance, whereas R_{ct1} and R_{ct2} denote the charge transfer resistance at the counter and the working electrodes, respectively. The constant phase elements of the counter and working electrodes are referred to as C_1 and C_2, respectively [69, 71]. It can be observed that the Nyquist plots include two semicircles: the first semicircle related to charge transfer at the counter electrode/electrolyte interface at a higher frequency, and the second semicircle attributed to the charge transfer at the working/electrolyte interface at a lower frequency than the smaller semicircles, suggesting a rapid transport of charge and more injected electrons transportation in the photocatalyst [72-75]. As seen from Table 1, the CuO/ZnO nanocomposite possesses lower electrochemical impedance to charge transfer than CuO and ZnO, which is associated with effective charge separation with faster charge transfer in CuO/ZnO nanocomposite [76, 77].

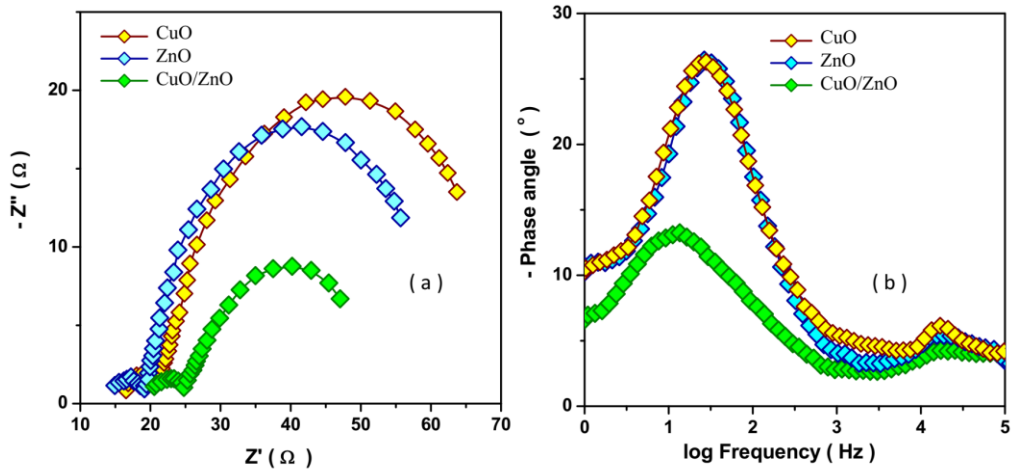

Figure 4. (a) Nyquist and (b) Bode plots of CuO, ZnO and CuO/ZnO nanocomposite in a 0.5 M Na_2SO_4 solution by applying an AC voltage of 10 mV in the frequency range from 10^{-2} Hz to 10^5 Hz at open circuit

Table 1. The obtained EIS parameters for CuO, ZnO and CuO/ZnO nanocomposite in a 0.5 M Na_2SO_4 solution.

Sample	Rs (Ω)	Rct_1 (Ω)	Rct_2 (Ω)
CuO	14.33	8.42	50.03
ZnO	14.91	4.89	43.55
CuO/ZnO	18.92	5.02	29.98

3.4. Study the photocatalytic performance

Figure 5 depicts the photodegradation efficiency of a blank sample (without photocatalyst), CuO, ZnO, and CuO/ZnO nanocomposite in removing 150 ml of a 100 mg/l RO16 solution under UV and sunlight irradiation. The degradation efficiency of the blank sample is 1.77% and 1.58% after 180 minutes of UV and sunshine light exposure, respectively, implying negligible degradation performance for the samples in the current photocatalysts. Figure 5a shows that after 125, 115, and 80 minutes of UV light exposure, 90% removal in the presence of CuO, ZnO, and CuO/ZnO nanocomposite is achieved, respectively. After 160, 135, and 120 minutes of UV light exposure, the dye is completely removed from CuO, ZnO, and CuO/ZnO nanocomposite, respectively. The observation indicated that the fast degaradation rate of dye under UV illumination occurs in the presence of CuO/ZnO nanocomposite because of the coupling of leaf-shaped CuO with rod-shaped ZnO which increases the electron hole separation and results in an improvement in photocatalytic activity. Furthermore, the formation of a heterostructure of nanostructured CuO-ZnO with a great specific surface area enhances optical absorption ability [78-80].

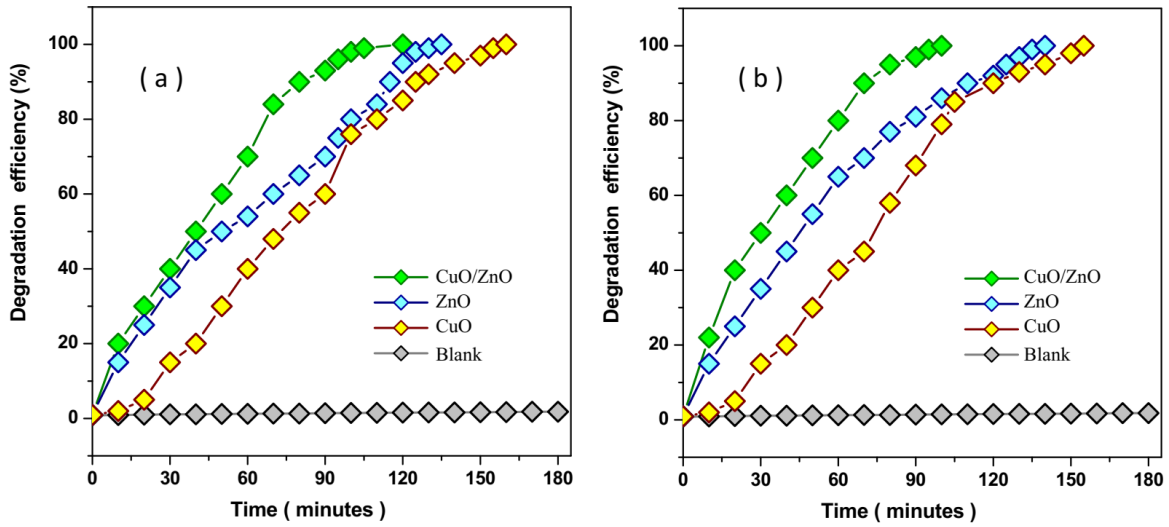

Figure 5. Photodegradation efficiency of blank sample (without photocatalyst), CuO, ZnO and CuO/ZnO nanocomposite to remove of 150 ml of 100 mg/l RO16 solution under (a) UV and (b) sunlight irradiations at λ_{max} = 493 nm at different intervals.

It is observed from Figure 5b after 120, 110 and 70 minutes of sunlight illumination, 90% dye removal is obtained in CuO, ZnO and CuO/ZnO nanocomposite, respectively. 100% removwal of dye is observed after 115, 140 and 100 minutes of sunlight illumination for CuO, ZnO and CuO/ZnO nanocomposite, respectively. Results indicate a higher degaradation rate of dye under sunlight than under UV illumination, which is attributed to band gap engineering and formation of interfacial contact between CuO and ZnO nanostructures in CuO/ZnO nanocomposite [81-83]. By absorbing photons under sunshine irradiation, oxygen defect states in CuO and ZnO nanostructures can be activated, promoting charge separation and facilitating electron transport from leaf-shaped CuO to rod-shaped

ZnO nanostructures. When a CuO/ZnO nanocomposite is exposed to sunlight, the CuO with a narrower band gap can operate as a sensitizer, absorbing visible light and promoting solar harvesting. The photo-excited electrons in CuO's valance band are injected into the conduction band at the same time as holes in the valance band are created, which can stay on the CuO surface and not migrate to ZnO's. Moreover, the photo-excited holes can migrate from valance band of ZnO to the valance band of CuO, which decreases the recombination of photo-excited electron-hole pairs in CuO/ZnO nanocomposite [84, 85]. Then, the photo-excited electrons are injected into the conduction band of ZnO [78, 86]. As expected, the injection of electrons from the conduction band of CuO into ZnO nanostructures and the trapping of electrons retard the back reaction between the photo-excited electrons and holes [87, 88]. These photo-excited charge carriers undergo the subsequent chemical reactions by generating the highly reactive species of reactive superoxide (O_2^-) radicals and hydroxyl radicals ($OH^\bullet$) from surface oxygen molecules which can destroy the adsorbed dye molecules on the surface of the photocatalyst [39, 89].

The photocatalytic performance of the CuO/ZnO nanocomposite is compared to that of other photocatalysts for RO16 degradation reported in the literature (Table 1). The CuO/ZnO nanocomposite exhibits efficient photocatalytic activity because the generated heterojunction nanocomposite between CuO and defect-rich ZnO nanostructures improves charge separation and life time of photo-excited charge carriers, displaying increased photocatalytic degradation of RO16.

Table 1. Comparison between the results of photocatalytic performance of CuO/ZnO nanocomposite with other photocatalysts reported in the literature for degradation of RO16.

Photocatalyst	**AO7 content (mg/l)**	**Light source**	**Degradation time (minute)**	**Removal efficiency (%)**	**Ref.**
TiO_2	61.7	UV	120	82	[30]
Ti/TiO_2	30	UV	20	100	[31]
TiO_2	20	UV	80	100	[32]
TiO_2	40	UV	30	95	[33]
CeO_2	50	UV	120	100	[34]
Irpex lacteus cultures immobilized on polyurethane foam	150	UV	1440	80	[35]
Nanostructure Cu–Zn mixed-oxide	11.3	UV–vis	120	20	[36]
Surfactant assisted TiO2	25	UV	120	40	[37]
CuO/ZnO nanocomposite	100	UV	120	100	Present study
		sunlight	100	100	

The photocatalytic performance of the produced photocatalysts was investigated in this work for the degradation of actual samples containing 150 ml of 100 mg/l RO16 solution made using textile wastewater from a textile plant in Shaoxing, Zhejiang, China, under sunlight irradiation. Figure 6 shows that 100% dye removal is achieved after 165, 155, and 112 minutes of solar illumination,

respectively, for CuO, ZnO, and CuO/ZnO nanocomposite, indicating a lower rate of dye degradation than the dye solution prepared with deionized water (Figure 5b). In genuine textile wastewater, it's linked to the presence of other pollutants [90], and the presence of colloidal particles in wastewater as light scattering agents which hinder the photocatalytic performance [91, 92]. Furthermore, these findings demonstrate the appropriate capability of CuO/ZnO nanocomposite to treat RO16 from textile wastewater.

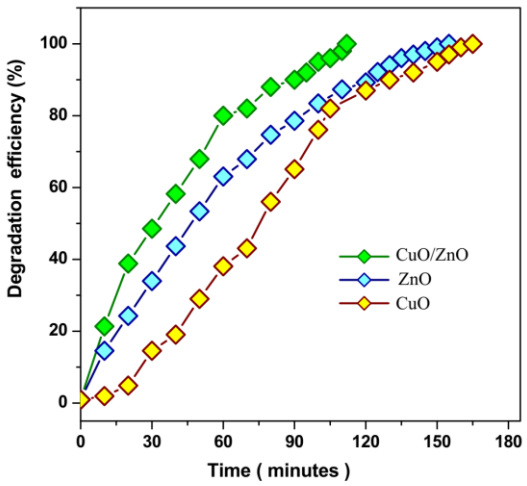

Figure 6. The degradation efficiency of CuO, ZnO and CuO/ZnO nanocomposite for degradation of 150 ml of 100 mg/l RO16 solution prepared using textile wastewater under sunlight irradiation at λ_{max} = 493 nm at different intervals.

4. CONCLUSION

The photo-electrocatalytic degradation of RO16 dye by CuO/ZnO nanocomposite under UV and sunlight irradiation for wastewater treatment was explored in this study. The CuO/ZnO nanostructure was synthesized using a hydrothermal technique. The creation of a monoclinic phase of leaf-shaped CuO loaded on a hexagonal wurtzite structure of rod-shaped ZnO was confirmed by studying the morphology and structure of the nanocomposite. The band gap energies of CuO, ZnO, and CuO/ZnO nanocomposite were determined to be 1.99, 2.19, and 3.34 eV, respectively, indicating that the decrease in band gap energy in CuO/ZnO nanocomposite toward ZnO was evidence of facilitation in photo-excitation of charge carriers utilizing low energy. According to an EIS investigation, the CuO/ZnO nanocomposite has a lower electrochemical impedance to charge transfer than CuO and ZnO, which is related to effective charge separation and faster charge transfer in CuO/ZnO nanocomposite. After 160, 135 and 120 minutes of UV light illumination for CuO, ZnO, and CuO/ZnO nanocomposite, respectively, total removal of 150 ml of 100 mg/l RO16 solution was achieved, and 100 percent dye removal was observed after 115, 140, and 100 minutes of sunlight light illumination for CuO, ZnO, and CuO/ZnO nanocomposite, respectively. The results show that dye degradation is faster when exposed to sunlight than when exposed to UV radiation, which can be related to band gap engineering and the creation of interfacial contact between CuO and ZnO

nanostructures in CuO/ZnO nanocomposite. The photocatalytic performance of the prepared photocatalysts in this study was investigated for degradation of actual samples under sunlight irradiation, which contained 150 ml of 100 mg/l RO16 solution prepared using textile wastewater from a textile plant in Shaoxing, Zhejiang, China, and results showed that total dye removal was achieved after 165, 155, and 112 minutes, respectively, for CuO, ZnO, and CuO/ZnO nanocomposite, which indicated a lower rate of dye degradation than that prepared dye solution with deionized water. Furthermore, these findings demonstrate the appropriate capability of CuO/ZnO nanocomposite to treat RO16 from textile wastewater.

References

1. A.S. Abdulhameed, A.H. Jawad and A.-T. Mohammad, *Bioresource technology*, 293 (2019) 122071.
2. Z. Zakaria, M.R. Othman, S.Z. Hasan and W.W. Ahmad, *Sains Malaysiana*, 48 (2019) 791.
3. L. Jiang, Y. Wang, X. Wang, F. Ning, S. Wen, Y. Zhou, S. Chen, A. Betts, S. Jerrams and F.-L. Zhou, *Composites Part A: Applied Science and Manufacturing*, 147 (2021) 106461.
4. M. Yang, C. Li, Y. Zhang, D. Jia, R. Li, Y. Hou and H. Cao, *The International Journal of Advanced Manufacturing Technology*, 102 (2019) 2617.
5. T.-H. Zha, O. Castillo, H. Jahanshahi, A. Yusuf, M.O. Alassafi, F.E. Alsaadi and Y.-M. Chu, *Applied and Computational Mathematics*, 20 (2021)
6. B. Zhou, Z. Liu, C. Li, M. Liu, L. Jiang, Y. Zhou, F.L. Zhou, S. Chen, S. Jerrams and J. Yu, *Advanced electronic materials*, 7 (2021) 2100233.
7. L. Zhang, L. Wang, Y. Zhang, D. Wang, J. Guo, M. Zhang and Y. Li, *Environmental research*, 206 (2022) 112629.
8. W. Liu, F. Huang, Y. Liao, J. Zhang, G. Ren, Z. Zhuang, J. Zhen, Z. Lin and C. Wang, *Angewandte Chemie*, 120 (2008) 5701.
9. Z.-R. Tan, Y.-Q. Xing, J. Cheng, G. Zhang, Z.-Q. Shen, Y. Zhang, G. Liao, L. Chen and S.-Y. Liu, *Chemical Science*, 13 (2022) 1725.
10. D. Jia, C. Li, Y. Zhang, M. Yang, X. Zhang, R. Li and H. Ji, *The International Journal of Advanced Manufacturing Technology*, 100 (2019) 457.
11. M. Nazeer, F. Hussain, M.I. Khan, E.R. El-Zahar, Y.-M. Chu and M. Malik, *Applied Mathematics and Computation*, 420 (2022) 126868.
12. S. Ren, B. Ye, S. Li, L. Pang, Y. Pan and H. Tang, *Nano Research*, 15 (2022) 1500.
13. C.-X. Chen, S.-S. Yang, J. Ding, G.-Y. Wang, L. Zhong, S.-Y. Zhao, Y.-N. Zang, J.-Q. Jiang, L. Ding and Y. Zhao, *Applied Catalysis B: Environmental*, 298 (2021) 120495.
14. H. Liu, X. Li, Z. Ma, M. Sun, M. Li, Z. Zhang, L. Zhang, Z. Tang, Y. Yao and B. Huang, *Nano Letters*, 21 (2021) 10284.
15. L. Zhang, Y. Xu, H. Liu, Y. Li, S. You, J. Zhao and J. Zhang, *Journal of Water Process Engineering*, 44 (2021) 102368.
16. C. Li, J. Li, S. Wang and Q. Zhang, *Advances in Mechanical Engineering*, 5 (2013) 986984.
17. M.A. Brown and S.C. De Vito, *Critical reviews in environmental science and technology*, 23 (1993) 249.
18. J. He, P. Xu, R. Zhou, H. Li, H. Zu, J. Zhang, Y. Qin, X. Liu and F. Wang, *Advanced Electronic Materials*, (2021) 2100997.
19. T.-H. Zhao, M.-K. Wang, G.-J. Hai and Y.-M. Chu, *Revista de la Real Academia de Ciencias Exactas, Físicas y Naturales. Serie A. Matemáticas*, 116 (2022) 1.
20. I. Arslan, I.A. Balcioğlu and D.W. Bahnemann, *Dyes and pigments*, 47 (2000) 207.

21. J.-W. Lee, S.-P. Choi, R. Thiruvenkatachari, W.-G. Shim and H. Moon, *Dyes and pigments*, 69 (2006) 196.
22. E. El-Ashtoukhy, A. Mobarak and Y. Fouad, *International journal of electrochemical science*, 11 (2016) 1883.
23. T.-H. Kim, C. Park, J. Yang and S. Kim, *Journal of hazardous materials*, 112 (2004) 95.
24. M.F. Abid, M.A. Zablouk and A.M. Abid-Alameer, *Iranian journal of environmental health science & engineering*, 9 (2012) 1.
25. R. Saratale, G. Saratale, J.-S. Chang and S. Govindwar, *Biodegradation*, 21 (2010) 999.
26. T.-H. Kim, C. Park and S. Kim, *Journal of Cleaner Production*, 13 (2005) 779.
27. T. Zhou, X. He, F. Song and K. Xie, *International journal of electrochemical science*, 11 (2016) 590.
28. R. Khosravi, H. Hossini, M. Heidari, M. Fazlzadeh, H. Biglari, A. Taghizadeh and B. Barikbin, *International journal of electrochemical science*, 12 (2017) 4745.
29. Y.-M. Chu, B. Shankaralingappa, B. Gireesha, F. Alzahrani, M.I. Khan and S.U. Khan, *Applied Mathematics and Computation*, 419 (2022) 126883.
30. H. Purnama, *Jurnal Teknik Gelagar*, 16 (2005) 85.
31. P.A. Carneiro, M.E. Osugi, J.J. Sene, M.A. Anderson and M.V.B. Zanoni, *Electrochimica Acta*, 49 (2004) 3807.
32. C.-Y. Chen, *Water, Air, and Soil Pollution*, 202 (2009) 335.
33. I. Poulios and I. Aetopoulou, *Environmental Technology*, 20 (1999) 479.
34. H. Balavi, S. Samadanian-Isfahani, M. Mehrabani-Zeinabad and M. Edrissi, *Powder technology*, 249 (2013) 549.
35. K. Svobodová, M. Senholdt, Č. Novotný and A. Rehorek, *Process Biochemistry*, 42 (2007) 1279.
36. M.H. Habibi and B. Karimi, *Spectrochimica Acta Part A: Molecular and Biomolecular Spectroscopy*, 124 (2014) 629.
37. S.R. Patil, U. Akpan and B. Hameed, *Desalination and Water Treatment*, 53 (2015) 3604.
38. H. Yan, M. Zhao, X. Feng, S. Zhao, X. Zhou, S. Li, M. Zha, F. Meng, X. Chen and Y. Liu, *Angewandte Chemie*, (2022) 1.
39. L. Zhu, H. Li, Z. Liu, P. Xia, Y. Xie and D. Xiong, *The Journal of Physical Chemistry C*, 122 (2018) 9531.
40. X. Zhang, G. Zhou, H. Zhang, C. Wu and H. Song, *Transition Metal Chemistry*, 36 (2011) 217.
41. H.-H. Chu, T.-H. Zhao and Y.-M. Chu, *Mathematica Slovaca*, 70 (2020) 1097.
42. K. Chandrappa and T. Venkatesha, *Materials and corrosion*, 64 (2013) 831.
43. L. He, C. Yang, J. Ding, M.-Y. Lu, C.-X. Chen, G.-Y. Wang, J.-Q. Jiang, L. Ding, G.-S. Liu and N.-Q. Ren, *Applied Catalysis B: Environmental*, 303 (2022) 120880.
44. X. Wang, C. Li, Y. Zhang, W. Ding, M. Yang, T. Gao, H. Cao, X. Xu, D. Wang and Z. Said, *Journal of Manufacturing Processes*, 59 (2020) 76.
45. A. Shokri and M. Mehdipour Ghazi, *Advances in Environmental Technology*, 2 (2016) 11.
46. T.-H. Zhao, Z.-Y. He and Y.-M. Chu, *AIMS Mathematics*, 5 (2020) 6479.
47. P. Sathishkumar, R. Sweena, J.J. Wu and S. Anandan, *Chemical Engineering Journal*, 171 (2011) 136.
48. G. Li, S. Huang, N. Zhu, H. Yuan, D. Ge and Y. Wei, *Chemical Engineering Journal*, 421 (2021) 127852.
49. J. Liu, Q. Zhang, X. Tian, Y. Hong, Y. Nie, N. Su, G. Jin, Z. Zhai and C. Fu, *Chemical Engineering Journal*, 404 (2021) 127146.
50. H. Karimi-Maleh, H. Beitollahi, P.S. Kumar, S. Tajik, P.M. Jahani, F. Karimi, C. Karaman, Y. Vasseghian, M. Baghayeri and J. Rouhi, *Food and Chemical Toxicology*, (2022) 112961.
51. Y. Chu and T. Zhao, *Mathematical Inequalities & Applications*, 19 (2016) 589.

52. H. Ftouhi, Z. El Jouad, M. Jbilou, M. Diani and M. Addou, *The European Physical Journal Applied Physics*, 87 (2019) 10301.
53. D. Ge, H. Yuan, J. Xiao and N. Zhu, *Science of The Total Environment*, 679 (2019) 298.
54. M. Ramesh, *Water Practice & Technology*, 16 (2021) 1078.
55. M. Yang, C. Li, Y. Zhang, D. Jia, R. Li, Y. Hou, H. Cao and J. Wang, *Ceramics International*, 45 (2019) 14908.
56. H. Karimi-Maleh, C. Karaman, O. Karaman, F. Karimi, Y. Vasseghian, L. Fu, M. Baghayeri, J. Rouhi, P. Senthil Kumar and P.-L. Show, *Journal of Nanostructure in Chemistry*, (2022) 1.
57. M.-K. Wang, M.-Y. Hong, Y.-F. Xu, Z.-H. Shen and Y.-M. Chu, *Journal of Mathematical Inequalities*, 14 (2020) 1.
58. M. Hussain, Z.H. Ibupoto, M.A. Abbassi, A. Khan, G. Pozina, O. Nur and M. Willander, *Journal of Nanoelectronics and Optoelectronics*, 9 (2014) 348.
59. W. Liu, J. Li, J. Zheng, Y. Song, Z. Shi, Z. Lin and L. Chai, *Environmental Science & Technology*, 54 (2020) 11971.
60. J. Xu, W. Wang, S. Sun and L. Wang, *Applied Catalysis B: Environmental*, 111-112 (2012) 126.
61. T. Gao, C. Li, Y. Zhang, M. Yang, D. Jia, T. Jin, Y. Hou and R. Li, *Tribology International*, 131 (2019) 51.
62. H. Maleh, M. Alizadeh, F. Karimi, M. Baghayeri, L. Fu, J. Rouhi, C. Karaman, O. Karaman and R. Boukherroub, *Chemosphere*, (2021) 132928.
63. X. Zhang and A. Tang, *Materials Express*, 2 (2012) 238.
64. Y. Wang, C. Li, Y. Zhang, M. Yang, B. Li, L. Dong and J. Wang, *International Journal of Precision Engineering and Manufacturing-Green Technology*, 5 (2018) 327.
65. S. Rashid, S. Sultana, Y. Karaca, A. Khalid and Y.-M. Chu, *Fractals*, 30 (2022) 2240026.
66. J. Fang and Y. Xuan, *RSC advances*, 7 (2017) 56023.
67. S. Guo, C. Li, Y. Zhang, Y. Wang, B. Li, M. Yang, X. Zhang and G. Liu, *Journal of Cleaner Production*, 140 (2017) 1060.
68. M.A. Khan, N. Nayan, M.K. Ahmad and C.F. Soon, *Nanomaterials*, 10 (2020) 1298.
69. H. Karimi-Maleh, R. Darabi, M. Shabani-Nooshabadi, M. Baghayeri, F. Karimi, J. Rouhi, M. Alizadeh, O. Karaman, Y. Vasseghian and C. Karaman, *Food and Chemical Toxicology*, 162 (2022) 112907.
70. S.N. Hajiseyedazizi, M.E. Samei, J. Alzabut and Y.-m. Chu, *Open Mathematics*, 19 (2021) 1378.
71. W. Wang, S. Guo, I. Lee, K. Ahmed, J. Zhong, Z. Favors, F. Zaera, M. Ozkan and C.S. Ozkan, *Scientific reports*, 4 (2014) 1.
72. S.C. Pradhan and S. Soman, *Results in Surfaces and Interfaces*, 5 (2021) 100030.
73. A. Hezam, K. Namratha, Q. Drmosh, B.N. Chandrashekar, G.K. Jayaprakash, C. Cheng, S.S. Swamy and K. Byrappa, *Ceramics International*, 44 (2018) 7202.
74. X. Pan, Y. Zhao, S. Liu, C.L. Korzeniewski, S. Wang and Z. Fan, *ACS applied materials & interfaces*, 4 (2012) 3944.
75. F. Jin, Z.-S. Qian, Y.-M. Chu and M. ur Rahman, *Journal of Applied Analysis & Computation*, 12 (2022) 790.
76. J. Ângelo, P. Magalhães, L. Andrade and A. Mendes, *Applied Surface Science*, 387 (2016) 183.
77. J. Zhang, C. Li, Y. Zhang, M. Yang, D. Jia, G. Liu, Y. Hou, R. Li, N. Zhang and Q. Wu, *Journal of Cleaner Production*, 193 (2018) 236.
78. K. Sahu, A. Bisht, S. Kuriakose and S. Mohapatra, *Journal of Physics and Chemistry of Solids*, 137 (2020) 109223.
79. B. Li, C. Li, Y. Zhang, Y. Wang, D. Jia and M. Yang, *Chinese Journal of Aeronautics*, 29 (2016) 1084.

80. F. Wang, M.N. Khan, I. Ahmad, H. Ahmad, H. Abu-Zinadah and Y.-M. Chu, *Fractals*, 30 (2022) 2240051.
81. J. Singh and R.K. Soni, *Applied Surface Science*, 521 (2020) 146420.
82. C. Liu and J. Rouhi, *RSC Advances*, 11 (2021) 9933.
83. S.A. Iqbal, M.G. Hafez, Y.-M. Chu and C. Park, *Journal of Applied Analysis & Computation*, 12 (2022) 770.
84. F. Cao, T. Wang and X. Ji, *Applied Surface Science*, 471 (2019) 417.
85. K.A. Zahidah, S. Kakooei, M. Kermanioryani, H. Mohebbi, M.C. Ismail and P.B. Raja, *International Journal of Engineering and Technology Innovation*, 7 (2017) 243.
86. R. Saravanan, V. Gupta, E. Mosquera and F. Gracia, *Journal of Molecular Liquids*, 198 (2014) 409.
87. A. Yaghoot-Nezhad, M. Moradi, M. Rostami, I. Danaee and M.R. Khosravi-Nikou, *Energy & Fuels*, 34 (2020) 13588.
88. L. Nan, C. Yalan, L. Jixiang, O. Dujuan, D. Wenhui, J. Rouhi and M. Mustapha, *RSC Advances*, 10 (2020) 27923.
89. Y. Zhang, C. Li, D. Jia, B. Li, Y. Wang, M. Yang, Y. Hou and X. Zhang, *Journal of Materials Processing Technology*, 232 (2016) 100.
90. W.Z. Khan, I. Najeeb and S. Ishtiaque, *Int J Eng Sci*, 5 (2016) 61.
91. L. Jiang and K.-H. Choo, *Chemical Engineering Journal*, 288 (2016) 798.
92. D. Zhang, C. Li, Y. Zhang, D. Jia and X. Zhang, *The International Journal of Advanced Manufacturing Technology*, 78 (2015) 1275.